ISSN 0018-151X, High Temperature, 2018, Vol. 56, No. 3, pp. 410–417. © Pleiades Publishing, Ltd., 2018.
Original Russian Text © M.A. Pakhomov, V.I. Terekhov, 2018, published in Teplofizika Vysokikh Temperatur, 2018, Vol. 56, No. 3, pp. 431–438.

HEAT AND MASS TRANSFER AND PHYSICAL GASDYNAMICS

# Effect of Flow Swirling on Heat Transfer in Gas-Droplet Flow Downstream of Abrupt Pipe Expansion

**M. A. Pakhomov[a], * and V. I. Terekhov[a], ****

[a] *Kutateladze Institute of Thermophysics, Siberian Branch, Russian Academy of Sciences, Novosibirsk, 630090 Russia*

**e-mail: pakhomov@ngs.ru*

***e-mail: terekhov@itp.nsc.ru*

Received January 12, 2016

**Abstract**—The effect the flow swirl parameter on heat transfer in a gas-droplet flow is numerically modeled by the Euler approach. The gaseous phase is described by a system of 3D RANS equations with consideration of the back effect of particles on transfer processes in the carrier phase. The gaseous phase turbulence is calculated according to the Reynolds stress transport model with consideration of the dispersed phase effect on the turbulent characteristics. A rapid dispersion of droplets over the pipe cross section is observed in a nonswirling gas-droplet flow downstream of an abrupt pipe expansion. A swirling flow is characterized by a growing concentration of fine particles at the pipe axis due to the accumulation of particles in the zone of flow recirculation and to the turbophoresis force. In a swirling flow, the separated-flow region becomes significantly shorter (by almost a factor of two as compared to that in a nonswirling flow). It is shown that addition of droplets results in a significant growth of heat transfer intensity (by more than a factor of 2.5) in comparison with single-phase swirling flow.

**DOI:** 10.1134/S0018151X18020177

## INTRODUCTION

As is known [1–3], swirling single-phase flows are characterized by high local gradients of averaged and pulsation velocities and are accompanied by intricate hydrodynamic phenomena due to the effects of centrifugal and Coriolis forces. Swirling two-phase flows moving in a pipe or channel with an abrupt expansion are widely used to stabilize burning in industrial combustor chambers and find application in separators. Recirculation flow resulting from an abrupt expansion has a noticeable influence on the intensity of heat transfer processes and on the propagation of dispersed phase; it also has a significant effect on the separating two-phase flow structure [4–6]. The interaction between fine particles and gaseous phase turbulent vortices is an intricate process, which has not yet been fully studied [7–9]. Therefore, while swirling two-phase flows with the evaporating particles are widely used for various practical applications, the turbulent transfer processes in such flows remain studied to an insufficient extent.

In [10–13], the results from experimental and numerical investigations of swirling gas-droplet flows downstream of a channel's abrupt expansion are reported. The authors of [10, 11] carried out numerical simulation of swirling gas-droplet flows under different conditions, including atomized burning fuel particles. The authors of [10] developed an Euler model and compared the obtained numerical results with their own data obtained from experiments on studying the evaporation of fuel particles in swirling gas flow. The gaseous phase turbulence is described with a $k$–ε model that takes into account the influence of particles and the carrier flow swirling effects. The numerical results were found to be in good agreement with the data of measurements. In [11], swirling gas–droplet flow in a pipe with burning liquid fuel particles was simulated by the 3D RANS approach, and the effect the gas turbulence has on the droplet evaporation rate was shown. With the swirl parameters $S < 1$, this effect cannot be ignored at a distance away from the inlet section, and with this effect have to also be taken into account near the inlet section $S > 1$. The last decade has witnessed the Large Eddy Simulation (LES) method being increasingly more frequently used the simulation of such flows [10, 12]. This method enables to numerically analyze the intricate processes occurring in two-phase flows under conditions close to those existing in real combustion chambers. However, application of the LES approach, especially with consideration of the effect the dispersed phase has on subgrid stresses, involves the need to use high-performance supercomputers, a circumstance that limits the application of this approach in the performance of engineering calculations of swirling two-phase flows containing separated-flow regions and evaporating droplets.

The Second Moment Closure (SMC) models [15, 16] are a method in which the intricate mixing processes and the anisotropy of gas velocity pulsations in single-

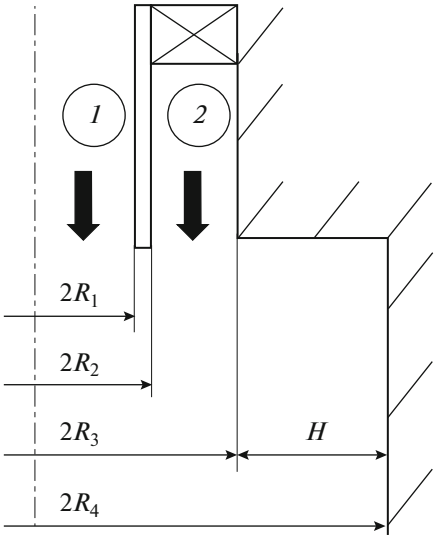


**Fig. 1.** Schematic diagram of the calculation region: (*1*) nonswirling gas-droplet flow; (*2*) swirling single-phase air flow.

phase separated swirling flows can partially be taken into account. In [6–18], successful application of the SMC models for two-phase flows was shown.

The goal of this study is to simulate numerically the effect of flow swirling on the dispersed phase distribution pattern and on heat transfer in gas-droplet flow downstream of an abrupt pipe expansion.

## PROBLEM STATEMENT AND THE NUMERICAL MODEL

We consider the dynamics of a swirling two-phase turbulent gas-droplet flow involving heat transfer with the channel walls. The problem is solved with the system of 3D Reynolds Averaged Navier-Stokes (RANS) equations with consideration of the back effect of particles on the transfer processes in gas. The analyzed flow is schematically shown in Fig. 1. The dispersed phase has a low volume concentration ($\Phi_1 = M_{L1}\rho/\rho_L < 2 \times 10^{-4}$). The particles are quite small in size ($d_1 < 100$ μm), due to which the effects caused by their collisions with one another can be disregarded. In this formula, $M_{L1}$ is the initial mass concentration of droplets, and ρ and $\rho_L$ are the densities of gas and droplets, respectively.

### *System of Averaged Gaseous Phase Equations*

In this study, we use the system of 3D RANS equations written in the cylindrical system of coordinates, which take into account the back effect of particles on the averaged and turbulent transfer processes in gas:

$$
\begin{gathered}
\rho\frac{\partial U_j}{\partial x_j} = \frac{6J}{d}\Phi, \\
\frac{\partial (U_iU_j)}{\partial x_j} = -\frac{\partial (P + 2k/3)}{\rho\partial x_i} + \frac{\partial}{\partial x_j}\left(\nu\frac{\partial U_i}{\partial x_j} - \langle u_iu_j\rangle\right) \\
- (U_i - U_{Li})\Phi\frac{\rho_L}{\rho}\left(\frac{1}{\tau} + \frac{6J}{\rho_L d}\right) + S_i, \\
\frac{\partial (U_iT)}{\partial x_j} = \frac{\partial}{\partial x_j}\left(\frac{\nu}{\mathrm{Pr}}\frac{\partial T}{\partial x_j} - \langle u_jt\rangle\right) \\
+ D_T\frac{(C_{PV} - C_{PA})}{C_P}\left(\frac{\partial K_V}{\partial x_i}\frac{\partial T}{\partial x_i}\right) \\
- \frac{6\Phi}{\rho C_P d}[\alpha(T - T_L) + JL], \\
\frac{\partial (U_iK_V)}{\partial x_j} = \frac{\partial}{\partial x_j}\left(\frac{\nu}{\mathrm{Sc}}\frac{\partial K_V}{\partial x_j} - \langle u_jk_V\rangle\right) + \frac{6J\Phi}{d}, \\
\rho = P/(R_gT).
\end{gathered}
\tag{1}
$$

In (1), $U_i$ ($U_Z \equiv U$, $U_r \equiv V$, $U_\varphi \equiv W$) and $u_i$ ($u_Z \equiv u$, $u_r \equiv v$, $u_\varphi \equiv w$) are the components of average velocity and of its pulsations; $x_i$ are projections on the coordinate axes; $\nu$ is the kinematic viscosity coefficient; $2k = \langle u_iu_i\rangle = u + v + w$ is the gaseous phase turbulence; $\tau = \rho_L d_1^2/(18\mu W)$ is the particle relaxation time with an accounting for deviation from Stoke's law $W = 1 + \mathrm{Re}_L^{2/3}/6$; $\mathrm{Re}_L = |\mathbf{U} - \mathbf{U}_L|d/\nu$ is the dispersed phase Reynolds number; $J$ is the mass flow of steam from the evaporating particle surface; $P$ is pressure; $S_i$ is the flow swirling influence factor ($S_U = 0$, $S_V = W^2/r - vV/r^2 + w^2/r$, $S_W = -VW/r - vW/r^2 + vw/r$) [15]; $T$ is temperature; $D_T$ is the turbulent diffusion coefficient; $C_P$ is the specific heat of gas; α is the evaporating droplet heat transfer coefficient; $L$ is the specific heat of vaporization; $K_V$ is the mass concentration of steam in a binary steam–gas mixture; $R_g$ is the specific gas constant; $\mathrm{Pr} = \nu/a$ and $\mathrm{Sc} = \nu/D$ are the Prandtl and Schmidt numbers, respectively; $a$ is thermal diffusivity, and $D$ is the diffusion coefficient. The subscripts $A$, $L$, $T$, and $V$ denote air, dispersed phase, turbulent parameter, and steam, respectively.

All equations of system (1) are written with consideration of the effect the presence and evaporation of a dispersed phase have on the momentum, heat, and mass transfer processes in a gas flow. The turbulent heat and diffusion fluxes in the gaseous phase are determined according to the Boussinesq hypothesis:

$$
\langle u_jt\rangle = -\frac{\nu_T}{\mathrm{Pr}_T}\frac{\partial T}{\partial u_j}, \quad \langle u_jk_V\rangle = -\frac{\nu_T}{\mathrm{Sc}_T}\frac{\partial K_V}{\partial u_j}.
$$

For the turbulent Prandtl and Schmidt numbers, it is assumed that $\mathrm{Pr}_T = \mathrm{Sc}_T = 0.85$.

*Reynolds Stress Transnport Model*

The gaseous phase turbulence was calculated with the elliptical Reynolds stress transfer model [16]:

$$\begin{aligned}
&\frac{\partial\left(U_j\left\langle u_i u_j\right\rangle\right)}{\partial x_j} = P_{ij} + \phi_{ij} - \varepsilon_{ij} \\
&+ \frac{\partial}{\partial x_l}\left(\frac{C_\mu T_T}{\sigma_k}\left\langle u_l u_m\right\rangle\frac{\partial\left\langle u_i u_j\right\rangle}{\partial x_m}\right) - A_d, \\
&\frac{\partial\left(U_j\varepsilon\right)}{\partial x_j} = \frac{1}{T_T}\left(C_{\varepsilon 1}P_2 - C_{\varepsilon 2}\varepsilon\right) \\
&+ \frac{\partial}{\partial x_l}\left(\frac{C_\mu T_T}{\sigma_\varepsilon}\left\langle u_l u_m\right\rangle\frac{\partial\varepsilon}{\partial x_m}\right) + \nu\frac{\partial^2\varepsilon}{\partial x_k\partial x_k} \\
&+ C_{\varepsilon 3}\nu\frac{k}{\varepsilon}\left\langle u_j u_k\right\rangle\left(\frac{\partial^2 U_i}{\partial x_j\partial x_l}\right)\left(\frac{\partial^2 U_i}{\partial x_k\partial x_l}\right) - \varepsilon_d, \\
&\beta - L_T^2\nabla^2\beta = 1/\left(\varepsilon T_T\right), \quad \phi_{ij} = \left(1-k\beta\right)\phi_{ij}^W + k\beta\phi_{ij}^H.
\end{aligned} \tag{2}$$

In [2], $P_{ij}$ is the energy transfer intensity from averaged to pulsation motion; $P_2 = 0.5P_{kk}$, $T_T = \max\left(k/\varepsilon; C_T\sqrt{\nu/\varepsilon}\right)$ is the turbulent time macroscale; $\phi_{ij}$ is the redistribution term describing the exchange of energy between individual components $\left\langle u_i u_j\right\rangle$ due to the pressure–deformation rate correlation; $\varepsilon$ is the energy dissipation or energy transfer rate from large-scale vortices to small-scale ones; $\beta$ is the mixing coefficient determined from the elliptical equation and used to calculate the redistribution term [16] (the value of which varies from zero at the wall to unity at a distance away from it); $\phi_{ij}^H$ is the "homogeneous" part of the redistribution term (at a distance away from the wall), and $\phi_{ij}^W$ is the "nonhomogeneous" part of the redistribution term (in the near-wall region). The redistribution term is written with consideration of the effect resulting from the flow being two-phase in nature [17]. The last terms $A_d$ and $\varepsilon_d$ on the right-hand sides of equations in system (2) take into account the back effect of particles on the carrier phase [6]:

$$A_P = \frac{2\rho_L\Phi}{\rho\tau}\left(1-f_u\right)\left\langle u_i u_i\right\rangle, \quad \varepsilon_P = \frac{2\rho_L\varepsilon}{\rho\tau}\left[\Phi\left(1-f_\varepsilon\right)\right],$$

where $f_u$ and $f_\varepsilon$ are the coefficients characterizing the involvement of particles in the turbulent motion of gas. The turbulence model constants and functions are given in [16]: $C_{\varepsilon 1} = 1.4$, $C_{\varepsilon 2} = 1.85$, $C_{\varepsilon 3} = 0.55$, $C_\mu = 0.22$, $\sigma_k = 1$, $\sigma_\varepsilon = 1.22$, and $C_T = 6$.

*System of Dispersed Phase Averaged Equations*

The system of averaged equations describing the transfer processes in the dispersed phase is given by

$$\begin{aligned}
&\frac{\partial\left(\rho_L\Phi U_{Lj}\right)}{\partial x_j} = -\frac{6J\Phi}{d}, \\
&\frac{\partial\left(\rho_L\Phi U_{Lj}U_{Li}\right)}{\partial x_j} + \frac{\partial\left(\rho_L\Phi\left\langle u_{Li}u_{Lj}\right\rangle\right)}{\partial x_j} \\
&= \Phi\left(U_i - U_{Li}\right)\frac{\rho_L}{\tau} + \Phi\rho_L g \\
&- \frac{1}{\tau}\frac{\partial\left(\rho_L D_{Lij}\Phi\right)}{\partial x_j} - \frac{\partial\left(\Phi P\right)}{\partial x_i}, \\
&\frac{\partial\left(\rho_L\Phi U_{Lj}T_{Li}\right)}{\partial x_j} + \frac{\partial}{\partial x_j}\left(\rho_L\Phi\left\langle\theta u_{Lj}\right\rangle\right) \\
&= \Phi\left(T_i - T_{Li}\right)\frac{\rho_L}{\tau_\Theta} - \frac{1}{\tau_\Theta}\frac{\partial\left(\rho_L D_{Lij}^\Theta\Phi\right)}{\partial x_j}.
\end{aligned} \tag{3}$$

In (3), $D_{Lij}$ and $D_{Lij}^\Theta$ are the tensors of turbulent diffusion and turbulent heat transfer of particles [18, 19], $\tau_\Theta = C_{PL}\rho_L d^2/\left(12\lambda Y\right)$ is the droplet thermal relaxation time, $Y = \left(1 + 0.3\,\mathrm{Re}_L^{1/2}\,\mathrm{Pr}^{1/3}\right)$, $C_{PL}$ and $\rho_L$ are the specific heat and density of droplet material.

The equations for calculating the second moments of dispersed phase velocity pulsations $\left\langle u_{Li}u_{Lj}\right\rangle$ are given in [18, 19]. The system of equations (1)–(3) is supplemented with the equation for heat transfer at the phase interface boundary (subject to the condition of the droplet temperature remaining constant over the droplet radius) and with the equation of steam mass conservation on the droplet's evaporating surface [6].

## NUMERICAL SOLUTION

The procedure for numerically implementing the Euler approach is described in detail in [6, 16]. The Reynolds stress components were determined according to [20] (Fig. 1). All calculations were carried out on a mesh 256 × 80 × 80 comprising around 1640000 control volumes. Attempts to further increase their number do not have any essential influence on the numerical calculation results.

At the pipe axis, the conditions of a smooth interface for both phases are specified, and the impermeability and no-slip conditions for the gaseous phase at the pipe wall are specified. For the dispersed phase at the channel wall, the "absorbing wall" boundary conditions are used [19], according to which a droplet coming in contact with the wall does return to the flow. According to the conditions specified in the outlet cross section, the derivatives of all sought parameters in the axial direction are taken to be equal to zero. The initial distributions of gas flow parameters were specified based on a preliminary calculation of single-phase flow in a pipe with the length equal to $150R$, where $R$ is the pipe radius. Thus, the gas flow moving in the inlet section has fully stabilized hydrodynamic parameters. A dispersed phase is added to

the air flow in the inlet section. For the dispersed phase, uniform distributions of the parameters over the pipe cross section were used. The initial values of the averaged radial phase velocities were determined with the use of the correlations for the solid body rotation law [21]:

$$V_1 = 4SU_1 r/R, \quad V_{L1} = 4S_L U_{L1} r/R,$$

$$S = \int_0^{R_3} \rho U_1 W_1 r^2 dr \Big/ R_3 \int_0^{R_3} \rho U_1^2 r dr,$$

$$S_L = \int_0^{R_3} \rho_L U_{L1} W_{L1} r^2 dr \Big/ R_3 \int_0^{R_3} \rho_L U_{L1}^2 r dr,$$

where $S$ and $S_L$ are the swirl parameters of air flow and dispersed phase, respectively.

At the first stage, the results obtained for a swirling single-phase air flow in a pipe with abrupt expansion [22] were compared. At the second stage, the results obtained for swirling flow of a mixture of air with solid particles without heat transfer between the phases were compared with the data of measurements given in [23, 24]. The comparison results are presented in [25]. Fairly good agreement was obtained between the calculated and measured data on the averaged and pulsation characteristics for both single-phase and two-phase turbulent flows (the difference did not exceed 15%), a circumstance that served as a basis for carrying out gas-droplet flow calculations using the Reynolds stress transfer model.

## NUMERICAL CALCULATION RESULTS AND THEIR ANALYSIS

Swirling gas-droplet two-phase flow was investigated in the down-flow mode in a abrupt pipe expansion (Fig. 1). Main jet *1* of a mixture of air and water droplets is supplied to the central pipe ($2R_1$). Swirling single-phase gas flow *2* enters through an annular channel ($R_3$–$R_2$). The calculation region geometrical parameters are as follows: $2R_1 = 20$ mm, $2R_2 = 26$ mm, $2R_3 = 40$ mm, $2R_4 = 100$ mm, and the step height $H =$ 30 mm. The calculation region length $X = 1$ m. The main air jet mass-average axial velocity $U_{m1} = 15$ m/s, and its mass flow rate $G_1 = 5.65$ g/s. The mass-average axial velocity and mass flow rate of air in the secondary annular jet $U_{m2} = 20.7$ m/s and $G_2 = 18$ g/s. The flow swirl parameter $S = 0$–$0.75$. The gaseous phase Reynolds number $\mathrm{Re} = U_{m1} 2R_1/\nu = 2 \times 10^4$. The initial averaged axial velocity of droplets $U_{L1} = 12$ m/s. The initial diameter of water droplets $d_1 = 10$–$100$ μm, and their mass concentration $M_{L1} = 0$–$0.1$. The particle relaxation time, which is written with consideration of the deviation from Stokes' power law $\tau = \rho_L d^2/(18\rho\nu W) = 0.3$–$30$ mm, where $W = 1 + \mathrm{Re}_L^{2/3}/6$. The wall temperature was constant over the entire calculation region length and equal to $T_W = \mathrm{const} = 373$ K. The temperature of air and droplets at the inlet $T_1 = T_{L1} = 293$ K. The Stokes number in the averaged motion $\mathrm{Stk} = \tau/\tau_f$, where $\tau_f$ is the turbulent time microscale, serves as the criterion characterizing the extent to which the particles are involved in the gaseous phase motion. It was shown earlier in [25] that low-inertia particles are involved in the gaseous phase separated motion with $\mathrm{Stk} \ll 1$ and that the dispersed phase does not participate in the recirculation motion with $\mathrm{Stk} \gg 1$. The dispersed phase passes through the shear flow region and does not enter the separated flow region almost at all. As a result, no change of turbulence is observed in the separation region, because there are almost no particles in it. In [4, 26], the following correlation for the dispersed phase relaxation time is given for nonswirling separated two-phase flows: $\tau_f = 5H/U_{m1} = 0.01$ s. Then, for the conditions of our calculations, we have $\mathrm{Stk} = 0.03$–$2.6$. The dispersed phase break up and coalescence effects are not considered due to the small quantity of particles. Droplets at the inlet are characterized by a monodisperse distribution. As the droplets move on along the pipe, droplet size is a variable quantity along all coordinates due to their heating and evaporation.

### *Distributions of Dispersed Phase Concentration*

Variations in the dispersed phase volume concentration along the pipe axis versus the droplet initial diameter, mass concentration of droplets, and swirl parameter S are given in Fig. 2, where $\Phi_0$ and $\Phi_1$ are the volume concentrations of particles at the pipe axis and in its inlet section, respectively. It should be pointed out that a uniform distribution of particle concentration along the pipe radius is specified at the calculation region inlet. In the case of nonswirled separated flow, the calculations were carried out with the total mass flowrate identical with that for the swirling flow.

Changes in the size of dispersed particles cause significant changes in the distribution of particle concentration in swirling separated flow (Fig. 2a). The volume concentration of the smallest particles (curve *1*, $d_1 = 10$ μm) rapidly decreases as a result of their being involved in the gaseous phase motion and are distributed over the channel's entire cross section, due to which they do not concentrate in the pipe near-axis region. For particles having larger inertia (curve *2*, $d_1 = 30$ μm), a very fast growth of dispersed phase concentration is observed in the initial cross sections due to its accumulation in the recirculation region under the effect of flow recirculation in the separation region. A nonuniform profile of the turbulent kinetic energy of gaseous and dispersed phases along the tube radius gives rise to turbulent migration of particles (a turbophoresis force) toward the pipe axis. This is why a maximum of droplet concentration appears at the channel axis when there are small particles. A feature characteristic of the most inertial particles (curve *3*, $d_1 = 100$ μm) investigated in this study is that the dis-

persed phase dissipates rapidly over the pipe cross section owing to the effect of centrifugal forces and due to turbulent diffusion and migration. These conclusions are consistent with the data obtained from measurements [23] and from numerical calculations carried out for swirling isothermal gas–dispersed flows downstream of an abrupt pipe expansion [24–26]. A change in the dispersed phase mass concentration has an effect on the distribution of the volume fraction of particles at the pipe axis in swirling flow (see Fig. 2b). Generally, the volume concentration profiles of particles in varying their initial fraction are qualitatively similar to each other.

The effect of flow swirling on the dispersed phase propagation over the pipe cross section is shown in Fig. 2c. For a nonswirling separated two-phase flow (dashed curve *1* at $S = 0$), rapid dispersion of droplets over the pipe cross section is observed, as a result of which their concentration decreases dramatically in the pipe near-axis region. A feature characteristic of swirling flow is that an increased quantity of small particles is observed at the pipe axis due to the effect of centrifugal and turbophoresis forces. This effect becomes more pronounced with increasing the swirl parameter (Fig. 2c), which is consistent with the data of calculations [25] for a confined swirling two-phase flow with solid particles. As the flow moves on along the tube length, the volume concentration of droplets in the near-axis region shows a very rapid decrease, which is attributed to the droplets being entrained from the near-axis region due to the effect of centrifugal forces. At a large distance ($x/H = 30$) from the pipe abrupt expansion section, the dispersed phase volume concentration at the pipe axis is almost zero.

The results from calculations aimed at analyzing the effect of flow swirling on the flow separation region length are shown in Fig. 3. Swirling has a significant effect on separated flow, and the recirculation zone length decreases (by almost a factor of two at $S = 0.5$) as compared with the case of nonswirling two-phase flow. It should be pointed out that changes in the mass concentration of droplets in the range $M_{L1} = 0.01$–$0.1$ causes the recirculation zone length to increase insignificantly by around 1%. This conclusion is consistent with the data obtained from the previous calculations of nonswirling gas–droplet flow downstream of an abrupt pipe expansion [6].

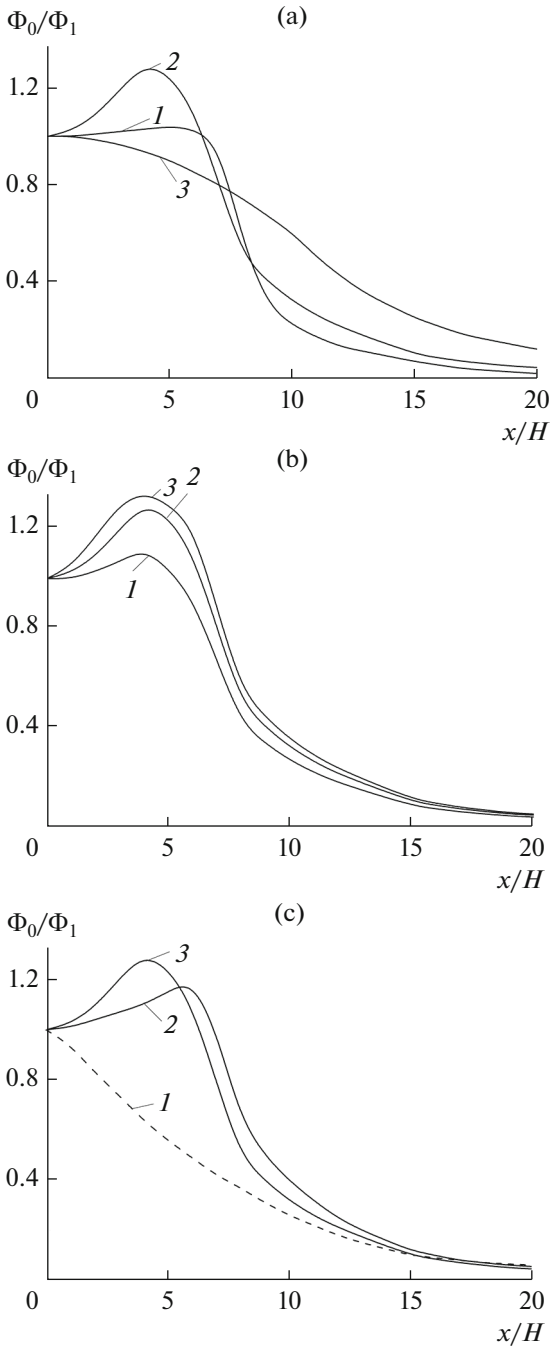


**Fig. 2.** Distributions of droplet volume concentration at the pipe axis in swirling flow for different sizes of particles (a), their mass concentration (b), and flow swirl parameter (c): (a) $M_{L1} = 0.05$ and $S = 0.5$; (*1*, *2*, and *3*) $d_1 = 10$, 30, and 100 μm. (b) $d_1 = 30$ μm and $S = 0.5$; (*1*, *2*, and *3*) $M_{L1} = 0.02$, 0.05, and 0.1. (c) $d_1 = 30$ μm and Stk = 0.26; (*1*, *2*, and *3*) $S = 0$, 0.25, and 0.5.

### *Heat Transfer*

Figure 4 shows distributions of the Nusselt number along the longitudinal coordinate in the swirling gas–droplet flow downstream of an abrupt pipe expansion for different values of initial droplet sizes and swirl parameter. The dashed curve shows the results of calculations carried out for the nonswirling separated single-phase flow at $S = 0$, and the solid curves show the results of calculations carried out for swirling single- and two-phase flows.

In the case of a single-phase flow, its swirling ($S = 0.5$) results in higher heat transfer in the recirculation zone as compared with a nonswirling separated flow (Fig. 4a). The Nusselt number values in the swirling flow relaxation region approximately correspond to its values for nonswirling separating flow. The addition of evaporat-

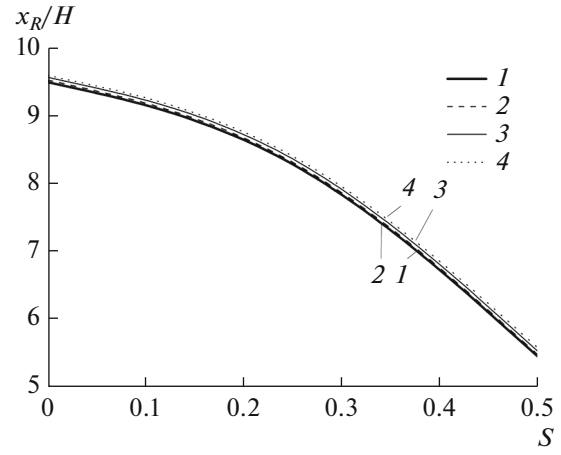


**Fig. 3.** Effect of the flow swirl parameter on the recirculation region length at $d_1 = 30$ μm and Stk = 0.26: (*1*) single-phase flow; (*2*, *3*, and *4*) $M_{L1} = 0.02$, 0.05, and 0.1.

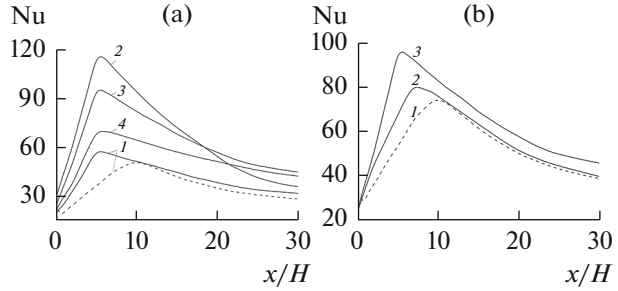


**Fig. 4.** Effect of initial droplet size (a) and flow swirl parameter (b) on heat transfer in swirling two-phase flow at $M_{L1} = 0.05$: (a) (*1*) single-phase flow; (*2*, *3*, and *4*) $d_1 =$ 10, 30, and 100 μm. (b) $d_1 = 30$ μm and Stk = 0.26; (*1*, *2*, and *3*) $S = 0$, 0.25, and 0.5.

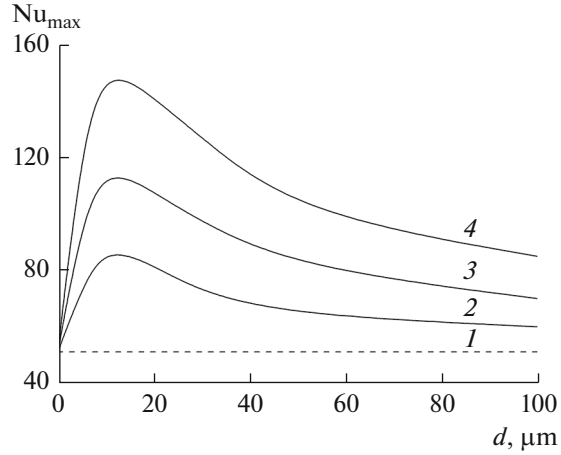


**Fig. 5.** Effect the addition of evaporating droplets on the maximal Nusselt number in swirling two-phase flow at $S = 0.5$: (*1*) single-phase flow; (*2*, *3*, and *4*) $M_{L1} = 0.02$, 0.05, and 0.1.

ing droplets causes the heat transfer to increase by almost a factor of two as compared with that in a swirling single-phase air flow (curve *1*). A change of the droplet initial diameter has an intricate effect on heat transfer in swirling flow. Initially, an increase in droplet size causes the heat transfer intensity to increase significantly due to evaporation of the dispersed phase in swirling flow ($d_1 = 10$ μm, curve *2*). This effect is noticeable at a short distance from the flow separation section ($x/H \le 5$). The heat transfer intensity shows a rapid decrease and tends to the corresponding value in a swirling single-phase flow. In the case of larger droplets ($d_1 = 30$ μm, curve *3*), the heat transfer intensity grows to a lesser extent, but this effect manifests itself over a longer pipe length. Droplets of the largest size investigated in this study ($d_1 = 100$ μm, curve *4*) are almost not involved in the gaseous phase motion at all and pass primarily through the flow core remaining almost beyond the recirculation near-wall region; these droplets intensify heat transfer primarily in flow relaxation region.

An increase in the flow swirl parameter entails an increase of heat transfer in the gas–droplet flow downstream of the abrupt pipe expansion (Fig. 4b). In a swirling flow, the point corresponding to the maximal heat transfer, which approximately coincides with the flow reattachment point, shifts upstream along the flow. This effect is intensified with increasing the swirl parameter, and, for $S = 0.5$, the separation region length in swirling flow is almost half that in nonswirling flow. In the range of small swirl parameter values $S = 0.25$ (curve *2*), heat transfer is intensified in the separation near-wall region, and its intensity in the flow restoration region is approximately equal to the value for the nonswirling separated single-phase flow.

The effect of the addition of droplets on the maximal heat transfer intensity in swirling flow is shown in Fig. 5, where $Nu_{0max} = 51.3$ is the maximal Nusselt number value in nonswirling separated flow ($S = 0$). The evaporation of droplets leads to a significantly higher heat transfer intensity in swirling two-phase flow (by more than a factor of 2.5 as compared with that in single-phase flow with the other parameters being the same). This effect becomes more pronounced with increasing the mass concentration of droplets. The diameter of dispersed phase particles has a more intricate effect on heat transfer. A drastic increase of heat transfer intensity is initially observed with an increase in the initial particle size. The region of the optimal initial droplet sizes lies in the interval of small droplet diameters ($d_1 \le 20$–$30$ μm) in the entire studied range of dispersed phase concentrations. After that, a significant decrease of heat transfer intensity is observed due to a significantly smaller phase interface area, and the maximal heat transfer tends to the corresponding value for the swirling single-phase flow.

## COMPARISON WITH THE MEASURED DATA

To carry out comparisons for the case of swirling gas–droplet flow downstream of an abrupt pipe expansion, we used the results obtained from LES simulations [13] and from experiments [27]. A swirling two-phase flow of a mixture of air and kerosene droplets was investigated in a horizontal flow downstream

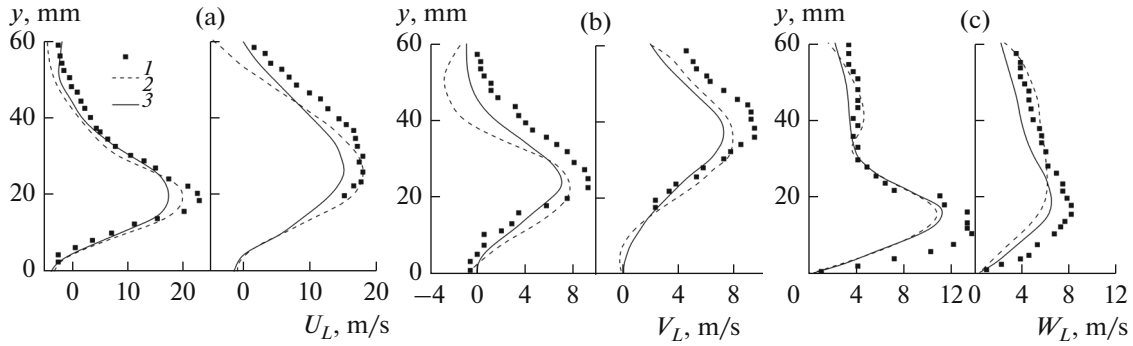


**Fig. 6.** The distributions of the averaged axial (a), transverse (b), and tangential (c) droplet velocities in swirling two-phase flow downstream of an abrupt expansion in a flat channel at the distance $x = 26$ mm (on the left) and 56 mm (on the right) at $d_1 = 55$ μm, Stk = 0.6, $M_L = 0.034$, and $S = 0.7$: (*1*) measured data of [27]; (*2*) data of LES Euler simulations from [13]; (*3*) data from the calculations carried out in this study.

of an abrupt channel expansion. The square-shaped channel had a height of 130 mm; its length was equal to 245 mm, and the step height $H$ was equal to 50 mm. Kerosene was supplied through a nozzle with the diameter $2R_1 = 5$ mm; air was supplied through a peripheral hole with the diameter $2R_3 = 30$ mm. The mass flowrate of gas $G_A = 15$ g/s, and that of the dispersed phase $G_L = 1$ g/s. The flow swirl parameter $S = 0.7$. The average initial air flow velocity $U_{m1} = 35$ m/s; the Reynolds number $\mathrm{Re} = U_m 2R_3/\nu = 7 \times 10^4$; the average droplet diameter in [13] $d$ was around 55 μm, and we used approximately the same size of droplets in this study. The inlet temperatures of air and kerosene droplets were $T_1 = 463$ K and $T_{L1} = 300$ K, respectively. The measurements reported in [27] were carried out with a phase Doppler anemometer. The data of experiments described in [27] at the distance $x = 6$ mm ($x/H = 0.12$) from the two-phase flow supply section were taken as the inlet distributions of the averaged and pulsation characteristics of both phases. The Stokes number in the averaged motion Stk = 0.6 and $\tau_f = 5$ ms. It points to the fact that the particles are readily involved in the turbulent gas motion [7, 25]. The profiles of three components of the kerosene droplet averaged velocity are shown in Fig. 6. The comparison results are shown in two sections at the distance from the flow separation point $x = 26$ mm ($x/H = 0.52$) and 56 mm ($x/H = 1.12$). The availability of a clearly pronounced maximum is characteristic of the droplet velocity longitudinal component (Fig. 6a). The dispersed phase velocity has a negative value in the pipe near-axis part, which means that droplets are entrained in the flow separation region. This result was obtained for both our calculations and for the measurements reported in [27] and for the LES calculations in [13]. The particle velocity transverse component is quite high, which is attributed to the presence of a back current region (Fig. 6b). The maximum in the distribution of the droplet circumferential velocity in the first section is due to the flow swirling effect (Fig. 6c). There is satisfactory agreement between the RANS-calculations carried out in this study and the data of the LES-simulations presented in [13] and the experiments of [27].

## CONCLUSIONS

Heat transfer in a swirling turbulent gas-droplet flow downstream of an abrupt pipe expansion has been simulated numerically using the Euler approach.

A rapid dispersion of droplets over the pipe cross section is observed in a nonswirling gas-droplet flow downstream of an abrupt pipe expansion. For a swirling flow, an increased concentration of fine particles at the pipe axis is typically observed, which is attributed to the effect of centrifugal and turbophoresis forces. It has been shown that large particles locate in the channel near-wall region due to the effect of centrifugal forces. Droplets that enter the near-axis separated flow region cannot escape from it, because the turbulence level in the shear layer is higher than it in the dispersed phase. The shear layer behaves as a barrier for the finely dispersed phase. In a swirling flow, the separated region becomes significantly shorter (almost half that in a nonswirling flow). This effect is amplified with increases in the flow swirl parameter; in parallel with this, the maximum of heat transfer intensity shifts toward upstream the flow. It has been shown that addition of droplets leads to a significant (by more than a factor of 2.5) enhancement of heat transfer in comparison with that in swirling single-phase air flow.

The obtained numerical calculation results have been compared with the experimental data in terms of the averaged characteristics of swirling turbulent gas–dispersed and gas-droplet flows downstream of an abrupt pipe expansion, including the droplet evaporation conditions. The calculated data are in fairly good agreement with the measured data for a confined swirling two-phase flow (the measured and calculated parameters differ from each other by no more than 15%).

## REFERENCES


1. Kutateladze, S.S., Volchkov, E.P., and Terekhov, V.I., *Aerodinamika i teplomassoobmen v ogranichennykh vikhrevykh potokakh* (Aerodynamics and Heat and Mass Transfer in Confined Vortex Flows), Novosibirsk: Inst. Teplofiz. Sib. Otd. Akad. Nauk SSSR, 1987.
2. Gupta, A.K., Lilley, D.G., Syred, N., *Swirl Flows*, Tunbridge Wells: Abacus, 1984.
3. Khalatov, A.A., *Teoriya i praktika zakruchennykh potokov* (Theory and Practice of Swirling Flows), Kiev: Naukova dumka, 1989.
4. Hishida, K., Nagayasu, T., and Maeda, M., *Int. J. Heat Mass Transfer*, 1995, vol. 38, p. 1773.
5. Senaha, I., Miyafuji, Y., Kato, S., Higa, M., and Yaga, M., *Trans. Jpn. Soc. Mech. Eng., B*, 2013, vol. 79, p. 1816.
6. Pakhomov, M.A. and Terekhov, V.I., *Int. J. Heat Mass Transfer*, 2013, vol. 66, p. 210.
7. Varaksin, A.Yu. and Zaichik, L.I., *High Temp.*, 1998, vol. 36, no. 6, p. 983.
8. Zaichik, L.I. and Varaksin, A.Yu., *High Temp.*, 1999, vol. 37, no. 4, p. 655.
9. Varaksin, A.Yu., *High Temp.*, 2015, vol. 53, no. 3, p. 423.
10. Klose, G., Schmehl, R., Meier, R., Maier, G., Koch, R., Wittig, S., Hettel, M., Leuckel, W., and Zarzalis, N., *J. Eng. Gas Turbines Power*, 2001, vol. 123, p. 817.
11. Sankaran, V. and Menon, S., J. Turbul., 2002, vol. 3, paper 011.
12. Sadiki, A., Chrigui, M., Janicka, J., and Maneshkarimi, M.R., *Flow, Turbul. Combust.*, 2005, vol. 75, p. 105.
13. Sanjose, M., Senoner, J.M., Jaegle, F., Cuenot, B., Moreau, S., and Poinsot, T., *Int. J. Multiphase Flow*, 2011, vol. 37, p. 514.
14. Durdina, L., Jedelsky, J., and Jicha, M., *Int. J. Heat Mass Transfer*, 2014, vol. 78, p. 892.
15. Jakirlic, S., Hanjalic, K., and Tropea, C., *AIAA J.*, 2002, vol. 40, p. 1984.
16. Manceau, R. and Hanjalic, K., *Phys. Fluids*, 2002, vol. 14, p. 744.
17. Beishuizen, N., Naud, B., and Roekaerts, D., *Flow, Turbul. Combust.*, 2007, vol. 79, p. 321.
18. Zaichik, L.I., *Phys. Fluids*, 1999, vol. 11, p. 1521.
19. Derevich, I.V., *High Temp.*, 2002, vol. 40, no. 1, p. 78.
20. Hanjalic, K. and Jakirlic, S., *Comput. Fluids*, 1998, vol. 27, p. 137.
21. Vinberg, A.A., Zaichik, L.I., and Pershukov, V.A., *Fluid Dyn. (Engl. Transl.)*, 1994, vol. 29, no. 1, p. 55.
22. Dellenback, P.A., Metzger, D.E., and Neitzel, G.P., *AIAA J.*, 1989, vol. 26, p. 669.
23. Sommerfeld, M. and Qiu, H.-H., *Int. J. Heat Fluid Flow*, 1991, vol. 12, p. 20.
24. Sommerfeld, M. and Qiu, H.-H., *Int. J. Multiphase Flow*, 1993, vol. 19, p. 1093.
25. Pakhomov, M.A. and Terekhov, V.I., *Therophys. Aeromech.*, 2015, vol. 22, no. 5, p. 597.
26. Fessler, J.R. and Eaton, J.K., *J. Fluid Mech.*, 1999, vol. 314, p. 97.
27. Garcia-Rosa, N., Phenomenes d'allumage d'un foyer de turbomachine en conditions de haute altitude, *Ph.D. Thesis*, Toulouse, France: Univ. Toulouse, Institut Superieur de l'Aeronautique et de l'Espace, 2008.


*Translated by V. Filatov*